Food Chemistry: X 24 (2024) 101906

Contents lists available at ScienceDirect

Food Chemistry: X

journal homepage: www.sciencedirect.com/journal/food-chemistry-x

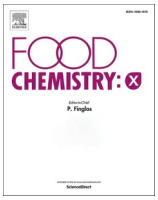

Prediction of 3D printability and rheological properties of different pineapple gel formulations based on LF-NMR

Yunfei Bao [a], Linlin Li [a,b,c,d,e,*], Junliang Chen [a,b,c], Weiwei Cao [a,b,c], Wenchao Liu [a,b,c], Guangyue Ren [a,b,c], Zhenjiang Luo [d], Lifeng Pan [d], Xu Duan [a,b,c,**]

[a] College of Food and Bioengineering, Henan University of Science and Technology, Luoyang 471023, China
[b] Agricultural Product Drying Equipment Engineering Technology Research Center in Henan Province, Henan University of Science and Technology, Luoyang 471023, China
[c] Agricultural Products Processing Equipment Engineering Research Center in Henan Province, Henan University of Science and Technology, Luoyang 471023, China
[d] R&D Center, Haitong Ninghai Foods Co., Ltd., Ninghai, Zhejiang, China
[e] School of Public Health, Qingdao University, Qingdao 266071, China

ARTICLE INFO

Keywords:
3D printability
Pineapple gels
Low-field nuclear magnetic resonance
Partial least squares
BP-ANN

ABSTRACT

In this study, a pineapple-starch-xanthan gum system was prepared using fresh pineapple juice, maize starch, and xanthan gum (XG). The feasibility of using low-field nuclear magnetic resonance (LF-NMR) to predict pineapple gels' rheological properties and printability was evaluated. Results indicated that as maize starch and XG increased, the gel transformed from unable to support printed models to a stable shape, eventually becoming too viscous for printing. Principal component analysis and Fisher discriminant analysis classified the gels into four categories based on their rheological properties, aligning with the actual printing results. Pearson correlation analysis showed a strong correlation between the LF-NMR parameters and the rheological properties of gels. The partial least squares (PLS) and back-propagation artificial neural network (BP-ANN) models constructed using the LF-NMR parameters can effectively predict the rheological properties of pineapple gels. Therefore, LF-NMR is a valuable, non-destructive method for quickly assessing pineapple gels' 3D printing suitability.

1. Introduction

3D printing, also known as additive manufacturing, is a technology that uses computer-aided design software to control and instruct digital manufacturing machines to create three-dimensional objects by adding material layer by layer (Fahmy et al., 2020). A lot of research is currently being done on the 3D printing of various food materials. 3D food printing technology based on fruit and vegetable raw materials can, not only take advantage of the nutritional properties of fruits and vegetables but also enable personalized customization of food products in terms of appearance and nutrition (Piyush Kumar & Kumar, 2020). Pineapple, a tropical fruit with a unique flavor and sweetness, contains a significant amount of bioactive compounds, fiber, minerals, and nutrients. It has anti-inflammatory, antioxidant, monitoring nervous system function, and bowel movement-promoting properties (Ali et al., 2020). Despite these health benefits, the sour taste and rough flesh of pineapple affect the taste. The use of 3D printing technology can make the texture of pineapple soft while maintaining its nutritional value. However, pineapple's high water content, low viscosity, and high fluidity after pulping do not meet the basic requirements for 3D printing materials.

Hydrocolloids have been widely used as thickeners for 3D printing of various printing systems based on fruit juice, such as lemon juice (Yang et al., 2017), mango juice concentrate (Yang et al., 2018), and strawberry juice (Liu, Bhandari, Prakash, et al., 2018). Commonly used hydrophilic food thickeners include starch, gelling gum, XG, cellulose, and cellulose derivatives (Saha & Bhattacharya, 2010). Starch is widely used in 3D printing due to its viscoelastic properties and ability to exhibit the rheological behavior of shear-thinning and thixotropic non-Newtonian pseudoplastic fluids (Maniglia et al., 2020). As an edible gum, XG can be used to modulate and improve the texture, flowability, and stability of food products. In 3D printing, XG has been shown to reduce the extrusion hardness and improve the printing and mechanical properties of the printed material (Jeon et al., 2023). In addition, XG can modulate the network structure, rheological properties, texture, and stability of

* Correspondence to: College of Food and Bioengineering, Henan University of Science and Technology, Luoyang, 471023, China.
** Correspondence to: College of Food and Bioengineering, Henan University of Science and Technology, Luoyang 471000, China.
E-mail addresses: linlinli2020@126.com (L. Li), duanxu_dx@163.com (X. Duan).

https://doi.org/10.1016/j.fochx.2024.101906
Received 1 September 2024; Received in revised form 3 October 2024; Accepted 14 October 2024
Available online 16 October 2024

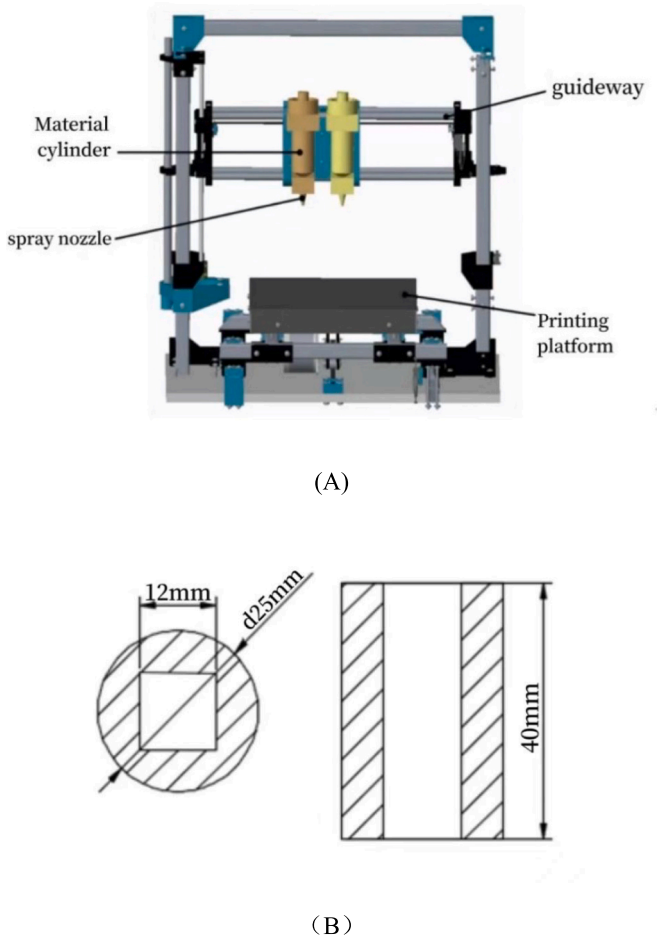

Fig. 1. Schematic diagram of Food Bot 3D printer structure (A), Schematic diagram of 3D printed model (B).

starch gels to improve the precision of 3D printing (Liu, Zhang, & Bhandari, 2018; Yu et al., 2022). As a result, XG is often used to improve the 3D printing properties of pure starch and other materials. Overall, it is possible to produce printable pineapple gels by adding starch and XG. For example, Azam et al. (2018) achieved 3D printing based on vitamin D-rich orange juice by adding starch and edible gum. Yu et al. (2022) found that adding different ratios of XG and acacia bean gum to potato starch could improve the mechanical strength and printing precision of the starch.

Based on previous research on extrusion-based 3D printing, the suitability of gels for this method is closely linked to rheological properties. The viscosity of the gel determines how difficult it is to extrude from the syringe (Zhu et al., 2019). The modulus of storage (G') and complex modulus (G*) correspond to the elasticity and rigidity of the gel and the stability after extrusion (Liu, Bhandari, Prakash, et al., 2018). It is essential to consider rheological properties when selecting gels for 3D printing. However, rheological testing is time-consuming and destructive. Rapid access to these rheological parameters could minimize the necessary experimentation when evaluating several materials suitable for 3D printing.

Low-field nuclear magnetic resonance (LF-NMR) is a rapid, non-destructive test that monitors the state and content of water in a sample's tissue. It does this by exploiting the differences in transverse relaxation time (T2) and relaxation peak area of different hydrogen protons in a radio frequency field (Chen et al., 2017). Significant correlations have been found between LF-NMR parameters and physical characteristic parameters of food. For example, Zhang et al. (2021) reported that LF-NMR combined with partial least squares regression can characterize the quality and physicochemical properties of fish under different frying conditions. Luo et al. (2020) found that LF-NMR and magnetic resonance imaging were effective in evaluating the gel properties of hairtail surimi with potato starch. Gao et al. (2020) have demonstrated that LF-NMR can evaluate ink water retention and ink quality.

Previous studies on 3D printability prediction have been limited to pure starch (Liu et al., 2020) or pure edible gum (Guo et al., 2020) systems. Most research on fruit-based systems has focused on 3D printability formulations. There are few studies on the 3D printability prediction of fruit-based systems. Therefore, in this experiment, the pineapple-maize starch-XG gel system was taken as the research object. Firstly, the printability and rheological properties of different formulations of pineapple gels were determined, and then the printability characteristics of pineapple gels were classified using principal component analysis (PCA) and Fisher's discriminant analysis. The moisture states of different gels were investigated by the LF-NMR technique. Finally, partial least squares (PLS) and BP-ANN models between LF-NMR parameters and the 3D printability of pineapple gels were developed.

2. Materials and methods

2.1. Materials

Grade B imported golden pineapple was purchased from Baiguoyuan in Luoyang, a Chinese fruit shop chain. Maize starch was purchased from the local Dazhang supermarket in Luoyang. XG was purchased from Yusuo Chemical Technology Co. Ltd., Shandong, China. The same batch of maize starch and edible gum was used throughout the experiment.

2.2. Sample preparation

The pineapple with a moisture content of 87 ± 0.2 % was washed and diced. It was mixed with 45 % (*w*/w) distilled water, pulverized for 10 min using a screw pulper, and sieved to remove the foam. Then maize starch was added at different levels of 15, 18, 21, 24, and 27 g /100 g pineapple juice, and then XG was added at different levels of 0.8, 1.0, 1.2, and 1.4 g /100 g pineapple juice. After mixing well, 100.00 g of weighed pineapple juice was added. Samples with varying levels of maize starch and XG are labeled as follows: samples A-E for maize starch (low to high) and samples 1–4 for XG (low to high).

The samples were homogenized for 5 min at 6400 rpm using a homogenizer (A25, Ouhe Machinery Equipment Co. Ltd., Shanghai, China). Next, the mixtures were heated at 85 ± 0.2 °C for 25 min. After cooling to room temperature, the samples were refrigerated at 4 °C. The samples were thawed to room temperature before printing. All measurements were completed within 48 h.

2.3. 3D printing experiment

In this study, a Food Bot 3D food printer (Hangzhou Shiyin Technology Co., Ltd., Zhejiang, China) (Fig. 1A) was used. The 3D model used is shown in Fig. 1B. The printing parameters were set as follows: nozzle diameter = 1.2 mm, infill percentage = 100 %, nozzle moving speed = 15 mm s^{-1}. The printing process was done at 25 °C. When the pineapple gel was deformed significantly during the printing process, the printing was stopped and the corresponding printing percentage was recorded. The printing percentage was obtained through the graphical user interface of the printer control software. Gels that achieved a 100 % printing percentage and maintained their intended shape without collapsing for 30 min at room temperature were considered to have good printability.

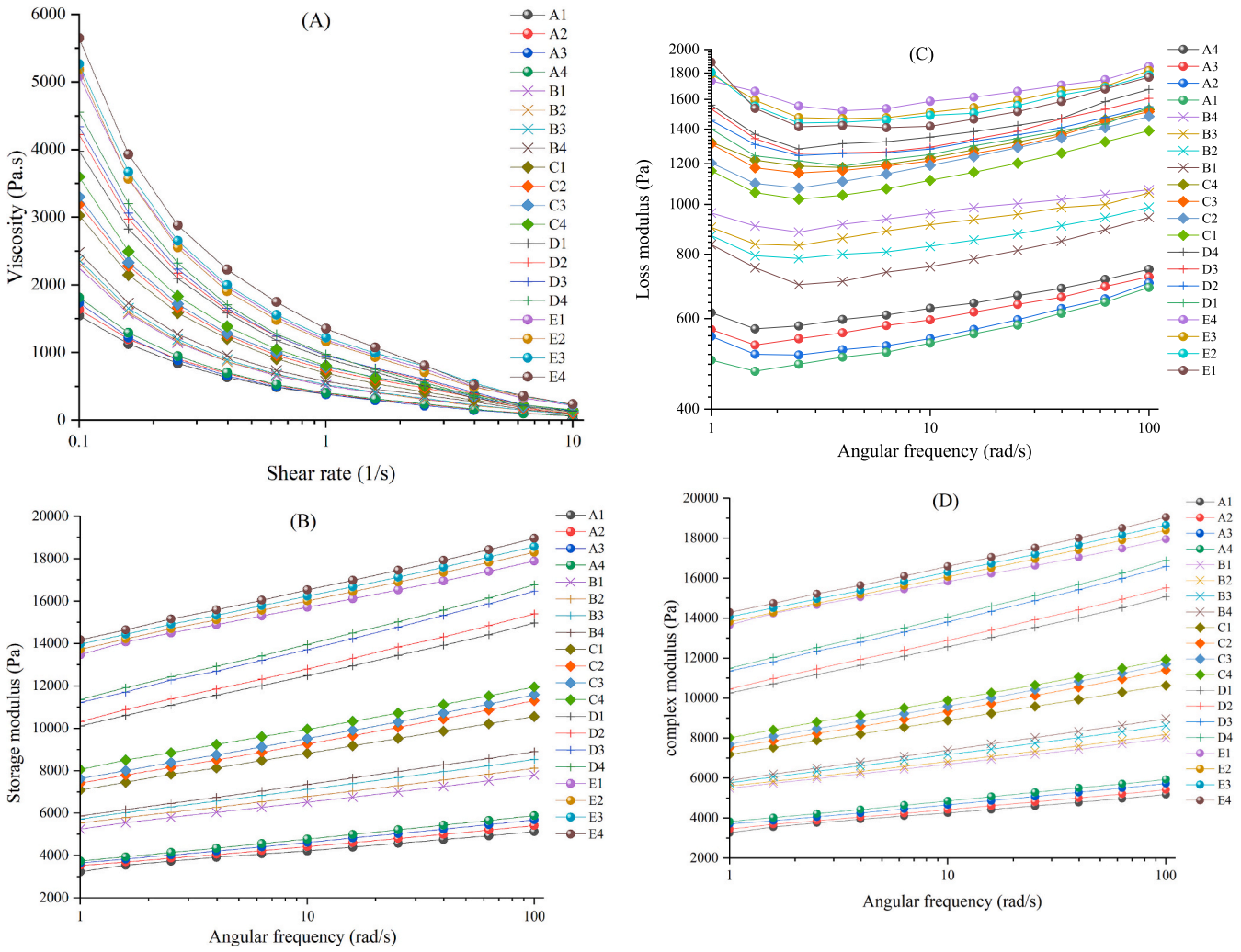

Fig. 2. Rheological properties of pineapple gels: Viscosity profiles (A); Storage modulus (B); C: Loss modulus (C); D: Complex modulus (D).

2.4. Rheological properties measurements

The rheological measurements were conducted using a rheometer (DHR-2, Shanghai Baosheng Industrial Development Co., Shanghai, China) with the application of a 40 mm parallel plate and a testing gap of 1000 μm. Viscosity values were recorded at 25 °C with a shear rate ranging from 0.1 to 10 s^{-1}. The dynamic viscosity values of different pineapple gels were then fitted by the power-law model, as follows:

$$\eta = K\gamma^{(n-1)} \quad (1)$$

where η indicates the viscosity (Pa·s), K indicates the consistency index (Pa·s^n), γ indicates the shear rate (s^{-1}), and n indicates the flow behavior index.

Oscillation frequency tests were conducted between 1 and 100 rad/s at a constant deformation of 0.1 % strain (within the linear viscoelastic range). All the experiments were conducted at 25 °C and repeated at least four times.

2.5. LF-NMR analysis

The transverse relaxation time (T_2) of pineapple gels was measured using an LF-NMR analyzer (MINI20-015 V-I, Shanghai Niumag Electronic Technology Co., Shanghai, China) with the magnet temperature of 32 °C. The analyzer was firstly calibrated by oil sample using the free induction decay (FID) method. Each sample consisted of 5.0 g of mixture wrapped in PE film and inserted into an NMR glass tube. The NMR probe was then inserted into the analyzer. Carr-Purcell-Meiboom-Gill (CPMG) sequences were used to measure spin-spin relaxation time. The parameters used in the CPMG sequence were set as follows: P1 (pulse time of 90°) =11.52 μs, P2 (pulse time of 180°) = 26 μs, TD (sampling point) = 149,992, SW (spectral width) =100 kHz, SF (spectrometer frequency) =21 MHz, NECH (number of echoes Echo Count) = 5000, NS (number of repeated scans) = 16, TW (time waiting) = 2000 ms. Continuous T_2 distribution profiles were obtained by analyzing the data acquired from the CPMG pulse sequence using the simultaneous iterative reconstruction technique (SIRT) algorithm. Each measurement was performed at least four times.

2.6. Data analysis

The 3D printability of different formulations of pineapple gels was analyzed by principal component analysis (PCA) and fisher discriminant analysis (FDA) based on rheological properties using SPSS 26.0 (IBM, Chicago, IL, USA). The 3D printability of the pineapple gels was classified using the rheological parameters (G', G", G*) and the consistency index (K). Pearson correlation analysis (PCA) was then performed to determine the correlation between G', G", G*, and K and the LF-NMR parameters. PLS modeling was performed using Unscrambler X 10.4. Of all the test data, 75 % of the dataset was used for training and 25 % for prediction. Rheological parameters were used as predictor variables (Y) and LF-NMR parameters as input variables (X). The BP-ANN

Table 1
Rheological parameters of different pineapple gels.

Samples	G'(Pa)	G" (Pa)	G*(Pa)	Power law		
				K(Pa·s^n)	n	R^2
A1	4224.23 ±151.96	537.61 ±42.28	4256.37 ±137.65	359.42 ±8.90	0.32 ± 0.01	0.998
A2	4419.41 ±179.32	548.48 ±34.88	4423.99 ±189.39	364.00 ±8.29	0.38 ± 0.01	0.998
A3	4618.83 ±71.75	596.31 ±14.80	4663.91 ±70.33	383.87 ±6.12	0.37 ± 0.01	0.999
A4	4778.33 ±106.68	628.17 ±44.90	4856.33 ±107.59	387.18 ±8.90	0.34 ± 0.01	0.998
B1	6511.16 ±199.27	757.06 ±67.47	6692.06 ±196.30	462.92 ± 12.26	0.34 ± 0.02	0.996
B2	6784.69 ±206.83	829.24 ±29.07	6831.94 ±208.09	474.13 ±17.50	0.33 ± 0.02	0.995
B3	7117.19 ±129.54	912.99 ±24.39	7175.35 ±128.87	497.29 ± 16.75	0.33 ± 0.02	0.996
B4	7345.05 ±175.12	960.91 ±44.37	7400.42 ±172.95	546.43 ± 20.30	0.36 ± 0.02	0.995
C1	8821.06 ±198.24	1113.87 ±108.71	8888.39 ±205.36	639.24 ±22.93	0.35 ± 0.01	0.998
C2	9260.78 ±161.49	1191.32 ±62.08	9340.13 ±162.79	664.69 ±11.61	0.36 ±0.02	0.996
C3	9513.15 ±110.23	1214.40 ±72.27	9600.18 ±115.54	708.91 ±23.86	0.36 ± 0.02	0.995
C4	9895.85 ±252.00	1230.22 ±89.60	9957.19 ±261.35	769.04 ±22.30	0.34 ± 0.02	0.996
D1	12,486.10 ±268.44	1249.44 ±91.14	12,574.00 ±260.87	860.77 ± 20.72	0.34 ± 0.01	0.998
D2	12,799.60 ±248.44	1281.35 ±69.52	12,893.28 ±256.62	905.42 ± 28.23	0.34 ± 0.02	0.997
D3	13,710.30 ±103.19	1291.41 ±38.44	13,808.70 ±106.72	918.80 ± 27.99	0.33 ± 0.02	0.997
D4	13,962.11 ±187.57	1351.03 ±62.58	14,060.61 ±190.39	962.09 ±28.81	0.31 ± 0.01	0.998
E1	15,704.90 ±238.12	1418.81 ±91.61	15,834.85 ±233.75	1080.61 ± 45.23	0.36 ± 0.02	0.995
E2	16,007.20 ±153.17	1489.37 ±82.89	16,070.60 ±156.40	1134.62 ± 45.14	0.35 ± 0.02	0.994
E3	16,241.60 ±165.94	1509.28 ±85.09	16,305.68 ±166.74	1170.67 ±33.78	0.33 ± 0.02	0.994
E4	16,528.90 ±178.70	1585.89 ±87.29	16,596.86 ±177.08	1225.54 ±47.72	0.36 ± 0.02	0.995

Note: G', G", and G* were recorded at 10 rad/s. K and n were achieved by fitting viscosity data to the Power Law equation.

technique was implemented in MATLAB R2019a (MathWorks Inc., Natick, MA, USA) with the hidden layers of 10. The network was trained using the Levenberg-Marquardt algorithm. LF-NMR parameters (20 × 4) were used as input data, and rheological parameters as output variables (1 × 80). The input data was randomly divided into 56 groups (70 %) for training, 12 groups (15 %) for validation, and 12 groups (15 %) for testing. The performance of the model was evaluated by calculating and comparing the following parameters:

$$RMSEC = \sqrt{\sum (y_{cal} - y_{act})^2 \Big/ n} \tag{2}$$

$$R_c^{\,2} = 1 - \frac{\sum (y_{cal} - y_{act})^2}{\sum (y_{cal} - y_{mean})^2} \tag{3}$$

$$RMSEC = \sqrt{\sum \left(y_{pre} - y_{act}\right)^2 \Big/ n} \tag{4}$$

$$R_p^{\,2} = 1 - \frac{\sum \left(y_{pre} - y_{act}\right)^2}{\sum \left(y_{pre} - y_{mean}\right)^2} \tag{5}$$

$$RPD = \frac{SD}{RMSEP} \tag{6}$$

where y_{cal} is calibrated value; y_{act} is the actual value; n is the number of samples; y_{mean} is the average value; y_{pre} is the predicted value; and *SD* is the standard deviation of the prediction set. R_c^2 is the coefficient of determination for the calibration data and R_p^2 is the coefficient of determination for the prediction data, *RMSEC* is the root mean square error for calibration and *RMSEP* is the root mean square error for prediction. The residual prediction deviation (*RPD*) was used to evaluate the regression performance of the three models.

Results are presented as means±standard deviation. The performance of the three models was assessed using Duncan's test and statistical differences between the means were determined at the 95 % confidence level. Data were plotted using Origin 2023 and the data were further analyzed.

3. Results and discussion

3.1. Rheological properties of pineapple gels

3.1.1. Viscosity of different pineapple gels

As shown in Fig. 2A, at the same shear rate, the viscosity of different types of pineapple gels increased with increasing levels of maize starch and XG. It also indicated that the starch content had a greater effect on the viscosity of the gels. This may be due to the slow leaching of amylose during the starch gelatinization process (water bath) and the extensive cross-linking of starch chains to form a dense cross-linked network structure. On the other hand, the increase of the content of short amylopectin after gelatinization is favorable to improving the density of the starch microstructure (Cheng et al., 2022). In addition, the starch content has a direct effect on the gel strength and apparent viscosity changes (Liu & Ciftci, 2020). XG can form intermolecular associations, resulting in the formation of a network structure of bound molecules (McClements, 2021; Sugiharto & Rahman, 2020). The combination of these factors resulted in an increase in the viscosity of the gels.

As the shear rate increased, the viscosity of the pineapple gel gradually decreased, exhibiting a shear thinning property. This may be because the network structure formed by the XG molecules was rapidly destroyed during shearing (Liu et al., 2021). This property facilitated the extrusion of the material and enhanced its static stability after extrusion (Wilson et al., 2017). The viscosity curves were fitted by the power law and the obtained fitting parameters of K and n are shown in Table 1. As the starch and XG content increased, the K value increased, indicating an increase in the viscosity of the gels (Guo et al., 2020). For example, the K values of the gels from formulations A1 to E4 were 359.417 ± 8.901 Pa·s^n to 1122.888 ± 40.017 Pa·s^n. However, K values should not be too high to obtain stable gel flow during printing. As expected, $n < 1$, indicating that all the gels were pseudoplastic fluids. The K values varied considerably between formulations, while n values varied insignificantly between formulations. It can be concluded that the main parameter influencing the apparent viscosity in this case is the K value.

3.1.2. Dynamic oscillation frequency analysis

As shown in Table 1, the storage modulus (G'), loss modulus (G"), and complex modulus (G*) of different formulations of pineapple gels at 10 rad/s were obtained. The G' measured the energy stored in the material during deformation and was an indicator of the material's elastic response. It reflected the material's ability to recover its original shape when stress was applied (Abdellatif et al., 2019). The G" measured the energy dissipated during deformation and was an indicator of the material's viscous response. It reflected the energy loss due to internal friction when stress was applied. The G* was a comprehensive indicator of the material's viscoelastic behavior, describing the total deformation response under dynamic stress (Klost & Drusch, 2019). Higher values of G' and G* indicated greater resistance to deformation and higher mechanical strength of the gel, while the G" reflected the extrudability through the nozzle (Liu et al., 2020). These parameters increased with

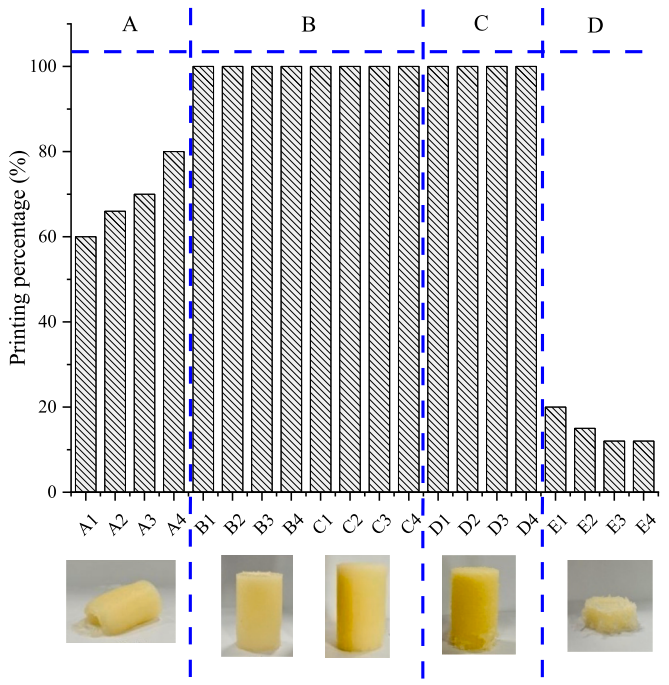

Fig. 3. Printing percentage and classification of different pineapple gels. A: unsupportable but flowable gels; B: supportable and flowable gels; C: supportable but less flowable gels; D: supportable but non-flowable gels.

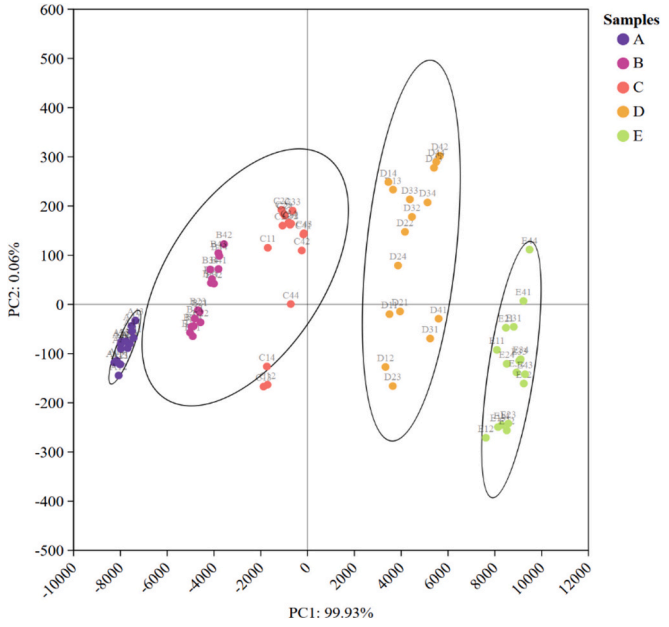

Fig. 4. Score plot of PCA analysis of rheological properties of pineapple gels (A1 in the symbol A1x represents formulation A1, x represents the number of parallel trials, and there are four parallels for each formulation. Other formulations are numbered according to the same criteria).

increasing angular frequency. According to Fig. 1 (B, C, and D), the G' values of all gels were found to be greater than their G" values. This suggested that the behavior of the pineapple gels was closer to that of elastic materials. The higher the values of G' and G*, the better the material's resistance to external deformation and support properties (Herranz et al., 2021; Liu et al., 2020). Furthermore, it was observed that G', G", and G* increased with increasing maize starch and XG content in the gels. This could be attributed to the higher solid content, which led

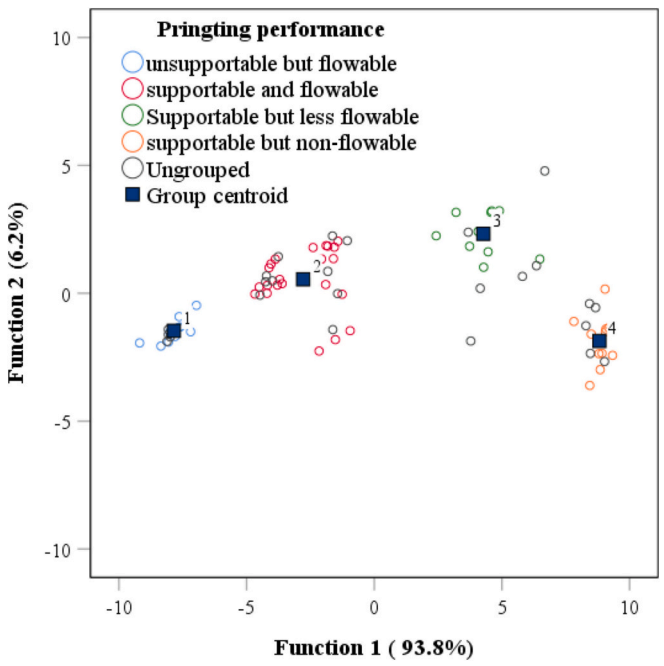

Fig. 5. Fisher discriminant analysis plot performed with the rheological data of pineapple gels.

to a thicker gel and reduced fluidity. Moreover, XG with trisaccharide side chains can form hydrogen bonds in aqueous solutions, providing more viscoelasticity to gels (Dick et al., 2020). Previous studies also showed that G', G" and viscosity of starch composite gels increased with increasing maize starch content (Cui et al., 2023). Similarly, Liu et al. (2021) found that the rheological parameters of mushroom gels increased with increasing XG content.

3.2. 3D printing performance

The 3D printing performance of different pineapple gels was evaluated based on the printing percentage of the model in Fig. 1B. The results are shown in Fig. 3. The addition of maize starch and XG had a significant effect on the 3D printing performance of the pineapple gels. When formulated as A1-A4, the pineapple gels did not achieve 100 % print completion and showed significant slump and skew (Fig. 3). As discussed in section 3.1.2, higher values of G', G*, and *K* indicate higher mechanical strength and better self-supporting ability of the gel, while a higher G" value indicates that the material is more difficult to extrude from the nozzle. From Table 1, it can be seen that G' (4224.230 ± 151.955–4778.331 ± 106.684 Pa), G* (4256.372 ± 137.648–4856.332 ± 107.592 Pa) and *K* (359.417 ± 8.901–387.183 ± 8.903 Pa·s^n) of pineapple gels in formulations A1-A4 were lower than those in other formulations. This indicated that the mechanical strength of pineapple gels in formulations A1-A4 was insufficient to support the weight of the material above them, resulting in poor printability. However, these gels had good flowability and were labeled as unsupportable but flowable gels. As the maize starch and XG content increased, as to formulations B1-B4 and C1-C4, the pineapple gels showed a 100 % printing percentage with clear lines and a fluent extrusion process. This was because the pineapple gels in these formulations had suitable G' (6511.157 ± 199.268–9895.846 ± 252.001 Pa), G* (6692.057 ± 196.297–9957.190 ± 261.34 Pa) and *K* values (462.918 ± 12.256–769.044 ± 22.301 Pa·s^n). This rheological property allowed the gels to be continuously extruded from the nozzle and had sufficient mechanical strength to effectively support multilayer stacked structures for 3D printing. The pineapple gels under these formulations (B1-B4 and C1-C4) were labeled as supportable and flowable gels.

Table 2
Classification of pineapple gels by Fisher discriminant analysis.

Formulation label	Calibration set						Prediction set					
	A	B	C	D	Total	Correctly classified (%)	A	B	C	D	Total	Correctly classified (%)
A1-A4	10				10	100	6				6	100
B1-C4		21	1		22	95.5		9	1		10	90
D1-D4			10		10	100			6		6	100
E1-E4				11	11	100				5	5	100
Total					53	98.9					27	97.5

A: unsupportable but flowable gels; B: supportable and flowable gels; C: supportable but less flowable gels; D: supportable but non-flowable gels.

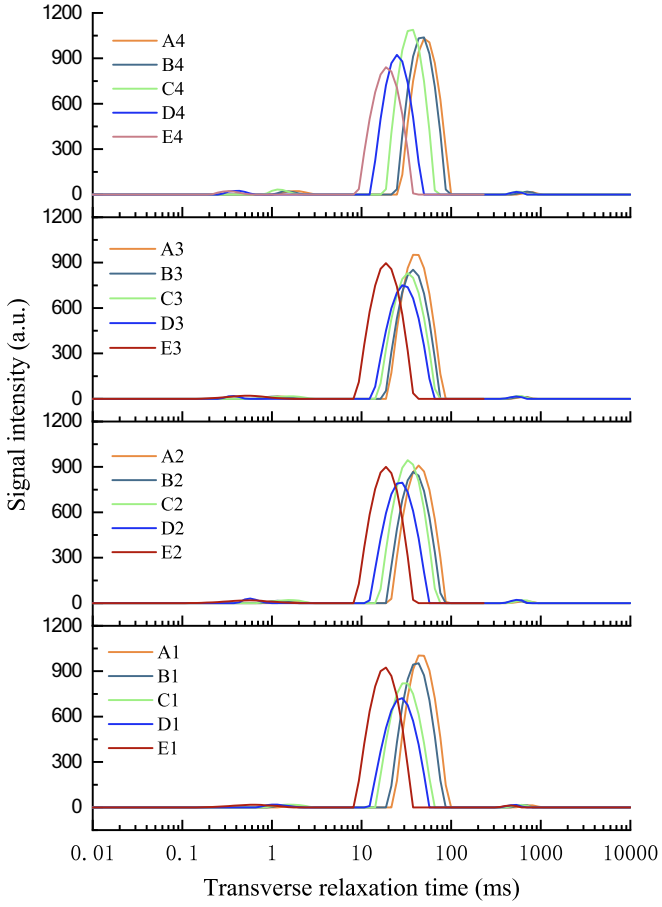

Fig. 6. T_2 curves of different pineapple gels.

However, when the starch content was increased to 24 g /100 g for formulations D1-D4, the extrusion of the pineapple gels became difficult. Some lines did not follow the intended trajectory, and the surface became rough. Nevertheless, the printing of the complete model could still be accomplished. This might be due to the higher viscosity (Fig. 1A) and yield stress (Fig. 1B) of these samples, which increased the extrusion difficulty and decreased the printing performance of the pineapple gels. The pineapple gels in these formulations were labeled as supportable but less flowable gels. When the maize starch addition was further increased (formulations E1 to E4 with maize starch addition of 27 g/100 g), the pineapple gels were essentially impossible to extrude and unable to complete the print. This was because the *K* value, representing the mechanical strength of the gels, was too high. The extrusion force of the printer could not reach the minimum force that could allow the gel to be continuously extruded, resulting in poor extrudability and line breakage after extrusion (Guo et al., 2021). Therefore, the pineapple gels under these formulations were labeled as supportable but non-flowable gels.

Based on actual printing, the printing behavior of pineapple gels can be classified into four categories: unsupportable but flowable gels (formulations A1-A4), supportable and flowable gels (formulations B1-C4), supportable but less flowable gels (formulations D1-D4), and supportable but non-flowable gels (formulations E1-E4).

3.3. Principal component analysis (PCA) based on rheological properties

From Section 3.2, it can be seen that the rheological data of different classified pineapple gels are within a certain range, respectively. To further understand the relationship between the rheological data G', G", G*, and *K* and the actual 3D printing results, the 3D printing behavior of pineapple gels was classified by PCA. Fig. 4 showed a plot of the scores on the PC1-PC2 axis, with a contribution of 99.93 % and 0.06 % for PC1 and PC2, respectively. A cumulative contribution of 99.99 % for PC1 and PC2 meant that these variables explained most of the information related to the 3D printing properties. On the PC1 axis, it was evident that the pineapple gels of all formulations were classified into four categories, which did not overlap with each other. Formulations A1-A4 were classified into a group corresponding to an unsupportable but flowable category, while formulations B1-C4 were classified into a group corresponding to a supportable and flowable category. Formulations D1-D4 fell into a group corresponding to a supportable but less flowable category, and formulations E1-E4 fitted into a group corresponding to a supportable but non-flowable category. This classification was consistent with the result in Fig. 3.

3.4. Fisher discriminant analysis (FDA) based on rheological properties

Fisher discriminant analysis is a statistical method for classifying the samples of unknown classes by training the samples that have been given the categories (Li et al., 2020). The basic idea is to project the multidimensional data in a certain direction to minimize the distance between the same classes. This way, the distance between different classes is maximized, allowing the samples to be best separated when projected in that direction. The rheological data such as G', G", G*, and *K* of pineapple gels were used as variables for discriminant analysis. 53 groups were randomly selected as training samples, while 27 groups were chosen as testing samples for discriminant analysis. As can be seen from Fig. 5, the distances between the four categories under the discriminant function were relatively far, indicating good classification. The classification accuracy of the calibration and prediction data was 98.9 % and 97.5 %, respectively (Table 2). The first type of classification was unsupportable but flowable gels with a classification accuracy of 100 %. The second classification type was supportable and flowable gels with 98.9 % classification accuracy for the validation set and 97.5 % classification accuracy for the prediction set. The third type was supportable but less flowable gels, and the fourth type was supportable but non-flowable gels, both with 100 % classification accuracy for the validation and prediction sets. The classification results of the Fisher discriminant analysis based on the rheological data of pineapple gels were also consistent with the actual 3D printing classification results.

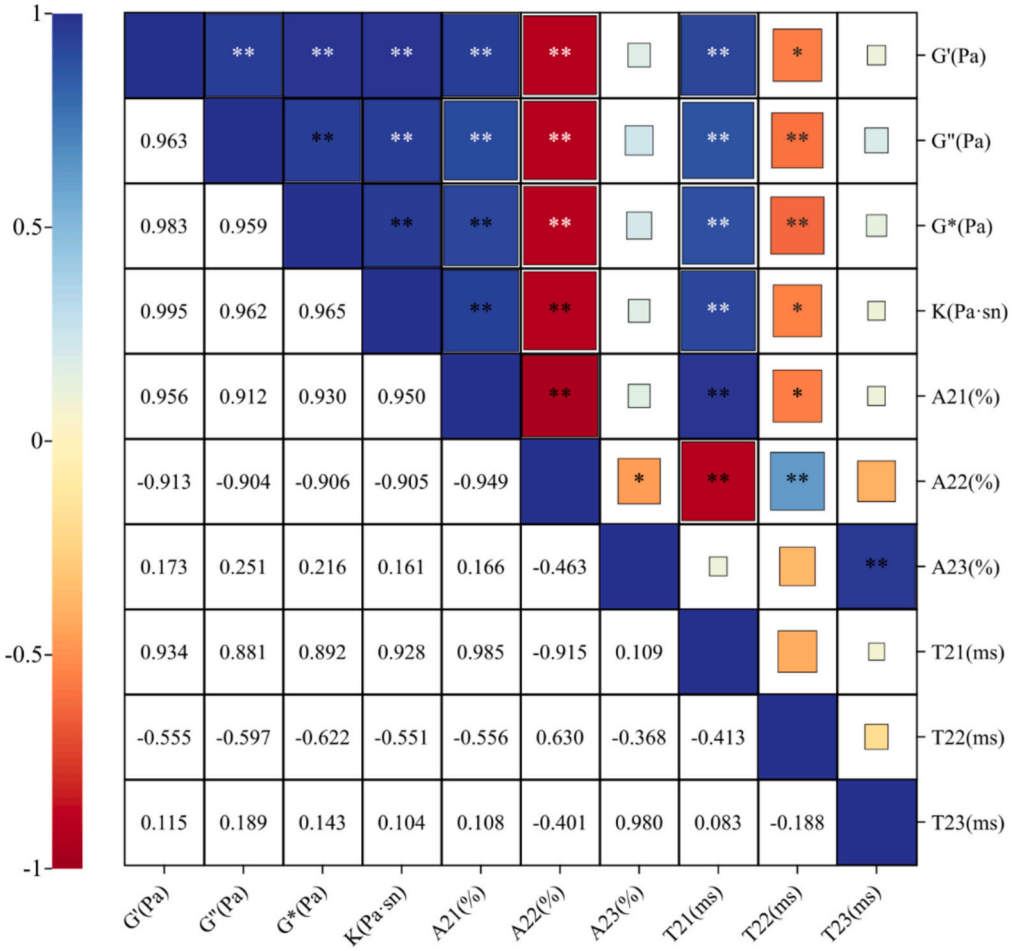

Fig. 7. Pearson correlation analysis between rheological parameters and LF-NMR parameters. (G': Storage modulus; G": Loss modulus; G*: Complex modulus; *K*: Consistency index. The symbol ** indicates a significant difference at $P < 0.01$. The symbol * indicates a significant difference at $P < 0.05$.)

Table 3
Performance parameters of PLS and BP-ANN models.

Rheological properties	Model	Calibration set		Validation set		Prediction set		*RPD*
		R_c^2	RMSEC	R_v^2	RMSEV	R_p^2	RMSEP	
G' (Pa)	PLS	0.953	907.161	0.942	1017.782	0.952	938.297	4.471
G" (Pa)		0.929	77.693	0.915	77.503	0.927	92.714	3.52
G*(Pa)		0.951	924.844	0.941	1034.618	0.954	929.971	4.508
K(Pa·s^n)		0.938	70.569	0.925	79.172	0.934	76.111	3.714
G' (Pa)	BP-ANN	0.998	223.906	0.970	629.243	0.980	649.220	6.348
G" (Pa)		0.994	24.901	0.991	40.370	0.982	43.288	7.277
G*(Pa)		0.997	286.304	0.992	384.154	0.987	533.243	7.843
K(Pa·s^n)		0.994	23.239	0.984	29.216	0.992	30.366	9.454

G': Storage modulus; G": Loss modulus; G*: Complex modulus; *K*: Consistency index.

3.5. LF-NMR analysis

Fig. 6 showed the variation in T_2 curves of different formulations of pineapple gels. In these curves, there were mainly three relaxation peaks, which were T_{21} (0.57–3.05 ms), T_{22} (18.73–49.77 ms), and T_{23} (351.11–905.48 ms). Typically, T_{21} represented tightly bound water associated with the gel structure. However, due to the very short relaxation time, hydrogen atom signals from solids (maize starch and XG) were also included. T_{22} represented weakly bound water, reflecting immobilized water molecules in the pineapple gel network. T_{23} represented free water, indicating the presence of freely movable water molecules within the gel network structure. All pineapple gels had the highest relaxation peak area (A_{22}) for weakly bound water. This indicated that the water state of pineapple gels in these experimental formulations was mainly weakly bound water. As the content of maize starch and XG increased, the T_2 curve shifted to the left with decreases in T_{21}, T_{22}, and T_{23}. This indicated a decrease in water molecular mobility in the pineapple gels. This decrease occurred because an increase in starch content formed a stronger gel network. An increase in XG created more polysaccharide linkages, forming a denser network structure with maize starch. Water molecules reoriented more slowly in this denser network because they were more tightly bound to the large biopolymer structures via hydrogen bonds. (Ozel et al., 2017). Additionally, it was observed that the area of the A_{22} relaxation peak gradually decreased while the area of the A_{21} peak increased. This change was attributed to the branching of XG molecules combining with the amylose in maize

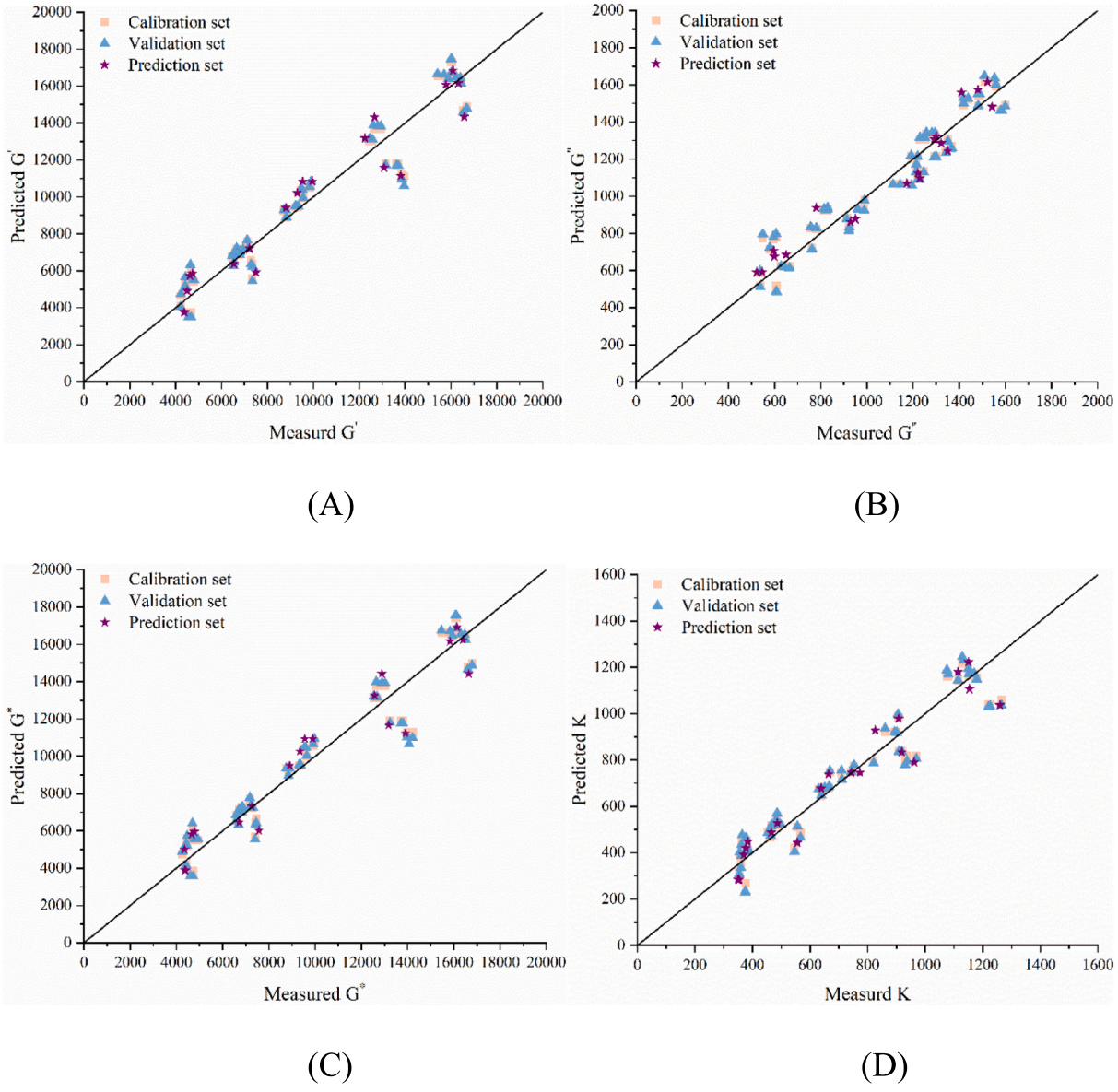

Fig. 8. Predicted rheological properties of pineapple gels based on LF-NMR parameters by PLS model. (A) Storage modulus (G'); (B) Loss modulus (G"); (C) Complex modulus (G*); (D) Consistency index (*K*).

starch. This combination hindered the rearrangement of amylose. Indirectly, it caused more hydroxyl groups in starch molecules to be exposed and interact with water molecules, leading to a decrease in A_{22} and an increase in A_{21} (Krystyjan et al., 2022). Furthermore, the solid matrix (maize starch and XG) itself contained a large number of hydrogen atoms, which also contributed to signal intensity (Kolehmainen, 2016). With the increase in XG and starch content, more water molecules were trapped in the dense gel network. This increased the number of restricted hydrogen atoms, collectively leading to an increase in the A_{21} peak area.

3.6. Correlation analysis between rheological parameters and LF-NMR parameters

To clarify the relationship between the LF-NMR properties and the rheological properties of the pineapple gels, a correlation analysis was performed and the results are shown in Fig. 7. Significant positive correlations were observed between the rheological parameters G', G", G*, and *K* with each other with correlation coefficients greater than 0.9. This indicated similar trends for these rheological parameters in pineapple gels under different formulations. However, A_{23} and T_{23} demonstrated low correlations with the rheological parameters, indicating that the rheological properties of different types of pineapple gels were less affected by the free water. In contrast, A_{21} and T_{21} showed highly significant positive correlations with the rheological parameters, with correlation coefficients ranging from 0.881 to 0.956. While A_{22} and T_{22} showed negative correlations with rheological parameters, with correlation coefficients ranging from −0.904 to −0.913 and − 0.551 to −0.612, respectively. The above results indicated that LF-NMR parameters had significant correlations with the rheological properties of pineapple gels to varying degrees. It was feasible to predict the rheological properties of pineapple gels using LF-NMR parameters.

3.7. Prediction of rheological parameters of pineapple gels based on PLS and BP-ANN models

The rheological properties have an important influence on the 3D printing properties of food materials. G' and G* are related to the

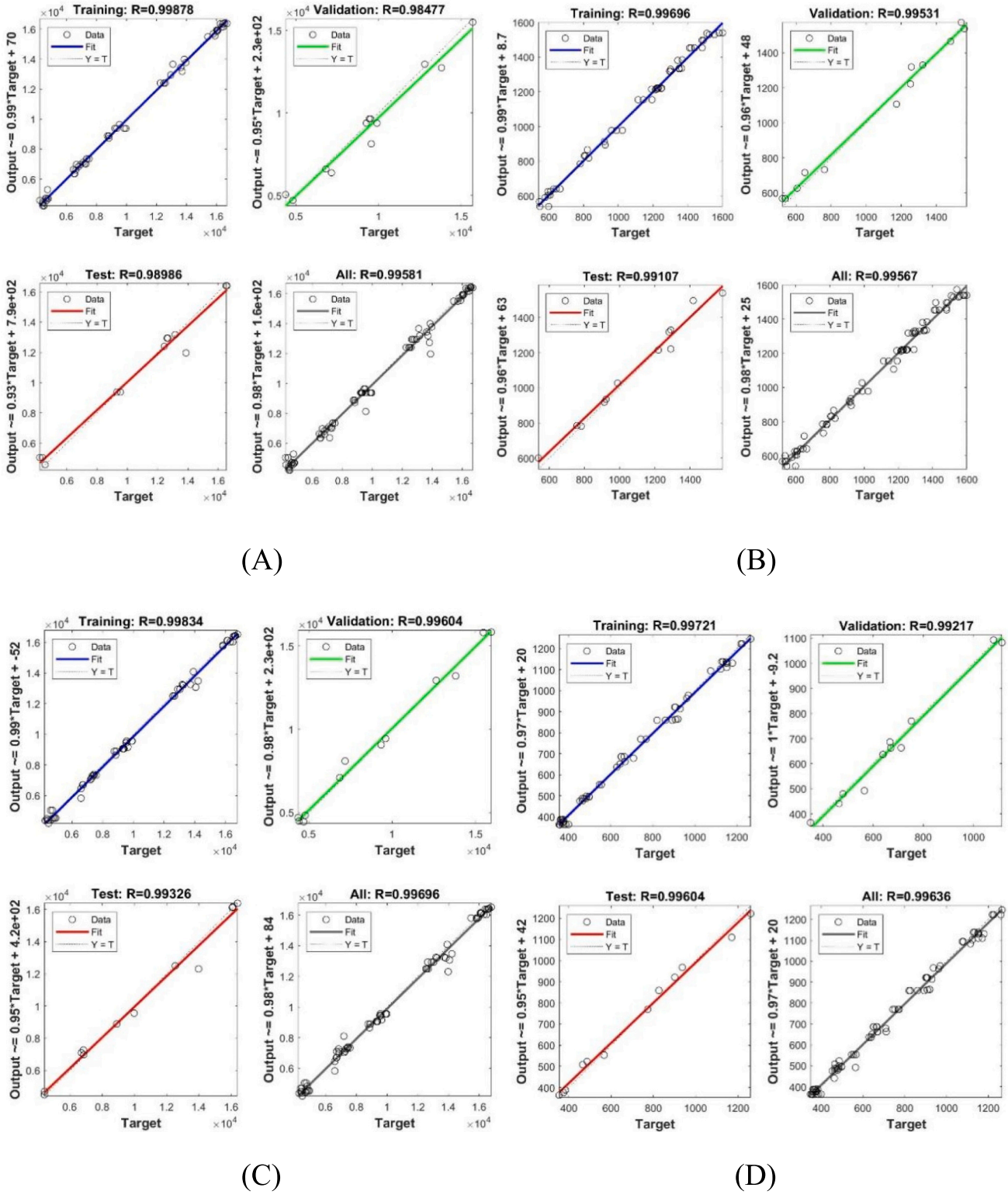

Fig. 9. Predicted rheological properties of pineapple gels based on LF-NMR parameters by BP-ANN model. (A) Storage modulus (G'); (B) Loss modulus (G"); (C) Complex modulus (G*); (D) Consistency index (*K*).

elasticity of the material, which reflects its ability to provide support and resist deformation during the printing material, and determines whether the pineapple gel of different formulations can complete the construction of the model. G" and *K* are related to the flowability of the material. The flowability of the printing material is reflected by the material's ability to flow under external extrusion, and is better when G" and *K* are smaller. Since the LF-NMR parameters A_{21}, T_{21}, A_{22}, and T_{22} were strongly correlated with the rheological parameters. This suggested that LF-NMR had the potential to predict the changes in G', G", G*, and *K*.

PLS is a linear modeling approach that correlates a predictor variable (Y-variable) with several dependent variables (X-variables) (Li et al., 2019). In this study, the rheological parameters (G', G", G*, and *K*) were

used as Y variables and the LF-NMR parameters (A_{21}, T_{21}, A_{22}, and T_{22}) were used as X variables to establish PLS models. The predictive performance of the model was assessed using R^2, RMSE, and *RPD* values as shown in Table 3. It can be seen that PLS models had a good predictive performance for G', G", G*, and *K* with R_p^2 values of 0.952, 0.927, 0.954, and 0.934, respectively. The *RPD* values were also above 3.0. The results suggested that LF-NMR could be used to predict the rheological properties of pineapple gels (Cascant et al., 2016). Fig. 8 showed the corresponding model in detail.

BP-ANN, a mathematical model simulating the neural feedback of the human brain, can self-learning, self-adaptation, and strong fault tolerance. It can deal with complex non-linear problems (Zhu et al., 2021). BP-ANN was used for modeling and the results are shown in Table 3 and Fig. 9. The R_C^2 and R_P^2 values for the calibration and prediction sets of G', G", G*, and *K* were very high, ranging from 0.980 to 0.998. The *RPD* values were 6.348, 7.277, 7.843 and 9.454, respectively. Higher R^2 and *RPD* values than PLS models proved that BP-ANN models had better prediction results. This indicated that the 3D printability of pineapple gels can be predicted by BP-ANN combined with LF-NMR parameters, with superior performance in prediction.

4. Conclusions

In this paper, we investigated the printing performance, rheological properties, and LF-NMR characteristics of pineapple gels with different contents of maize starch and XG. The actual printing results classified the pineapple gels into four categories: unsupportable but flowable gels, supportable and flowable gels, supportable but less flowable gels, and supportable but non-flowable gels. Based on the PCA analysis and Fisher discrimination of rheological properties, the pineapple gels could be accurately classified into four categories. And the classification results were consistent with the actual printing results. The prediction results showed that the PLS and BP-ANN models with LF-NMR parameters (A_{21}, T_{21}, A_{22}, and T_{22}) as input variables can accurately predict the rheological properties of pineapple gels. Therefore, the prediction of printability can be achieved by determining the class of pineapple gels through the ranges of rheological parameters obtained from the models. In conclusion, the feasibility of using LF-NMR to predict the rheological properties and printability of pineapple gels has been primarily confirmed.

CRediT authorship contribution statement

Yunfei Bao: Writing – original draft, Investigation, Data curation. **Linlin Li:** Writing – review & editing, Supervision, Investigation. **Junliang Chen:** Supervision, Project administration. **Weiwei Cao:** Writing – review & editing, Resources. **Wenchao Liu:** Writing – review & editing, Resources. **Guangyue Ren:** Supervision, Resources, Investigation. **Zhenjiang Luo:** Supervision, Funding acquisition. **Lifeng Pan:** Funding acquisition. **Xu Duan:** Supervision, Methodology, Investigation.

Declaration of competing interest

The authors declare that they have no known competing financial interests or personal relationships that could have appeared to influence the work reported in this paper.

Data availability

Data will be made available on request.

Acknowledgment

We acknowledge the financial support from National Key Research and Development Program of China (No. 2022YFF1101600), the Leading Talent Program for Science and Technology Innovation in Central China (No. 234200510020), Key Science and Technology Program of Henan Province (No. 232102111064, No. 232102110161), Natural Science Foundation of Henan (No. 232300420199), Key Scientific Research Projects of Henan Higher Education Institutions (No. 22A550005), Young Teacher Funding Program of the Henan Higher School (No. 2020GGJS072), and Special Program for the Introduction of Foreign Intelligence in Henan Province (Foreign Experts Project) (No. HNGD2023011), all of which enabled us to carry out this study.

Appendix A. Supplementary data

Supplementary data to this article can be found online at https://doi.org/10.1016/j.fochx.2024.101906.

References

Abdellatif, A., Hussain, S., Alamri, M., Qasem, A., Ibraheem, M., & Alhazmi, M. (2019). Dynamic rheological properties of corn starch-date syrup gels. *Journal of Food Science and Technology, 56*, 927–936. https://doi.org/10.1007/s13197-018-03558-9

Ali, M. M., Hashim, N., Abd Aziz, S., & Lasekan, O. (2020). Pineapple (Ananas comosus): A comprehensive review of nutritional values, volatile compounds, health benefits, and potential food products. *Food Research International, 137*, Article 109675. https://doi.org/10.1016/j.foodres.2020.109675

Azam, R. S. M., Zhang, M., Bhandari, B., & Yang, C. (2018). Effect of different gums on features of 3D printed object based on vitamin-D enriched Orange concentrate. *Food Biophysics, 13*, 250–262. https://doi.org/10.1007/s11483-018-9531-x

Cascant, M. M., Sisouane, M., Tahiri, S., El Krati, M., Cervera, M. L., Garrigues, S., & de la Guardia, M. (2016). Determination of total phenolic compounds in compost by infrared spectroscopy. *TALANTA, 153*, 360–365. https://doi.org/10.1016/j.talanta.2016.03.020

Chen, L., Tian, Y., Sun, B., Wang, J., Tong, Q., & Jin, Z. (2017). Rapid, accurate, and simultaneous measurement of water and oil contents in the fried starchy system using low-field NMR. *Food Chemistry, 233*, 525–529. https://doi.org/10.1016/j.foodchem.2017.04.147

Cheng, Y., Liang, K., Chen, Y., Gao, W., Kang, X., Li, T., & Cui, B. (2022). Effect of molecular structure changes during starch gelatinization on its rheological and 3D printing properties. *Food Hydrocolloids, 137*, Article 108364. https://doi.org/10.1016/j.foodhyd.2022.108364

Cui, Y., Yang, F., Wang, C.-s., Blennow, A., Li, C., & Liu, X. (2023). 3D printing windows and rheological properties for normal maize starch/sodium alginate composite gels. Food Hydrocolloids, 146, 109178. doi:https://doi.org/10.1016/j.foodhyd.2023.109178.

Dick, A., Bhandari, B., Dong, X., & Prakash, S. (2020). Feasibility study of hydrocolloid incorporated 3D printed pork as dysphagia food. *Food Hydrocolloids, 107*, Article 105940. https://doi.org/10.1016/j.foodhyd.2020.105940

Fahmy, A., Becker, T., & Jekle, M. (2020). 3D printing and additive manufacturing of cereal-based materials: Quality analysis of starch-based systems using a camera-based morphological approach. *Innovative Food Science & Emerging Technologies, 63*, Article 102384. https://doi.org/10.1016/j.ifset.2020.102384

Gao, C., Hou, X., Xing, T., & Chen, G. (2020). Development and design of low volatile waterborne disperse ink using LF-NMR. *Colloids and Surfaces A: Physicochemical and Engineering Aspects, 592*, Article 124503. https://doi.org/10.1016/j.colsurfa.2020.124503

Guo, C., Zhang, M., & Chen, H. (2020). Suitability of low-field nuclear magnetic resonance (LF-NMR) combining with back propagation artificial neural network (BP-ANN) to predict printability of polysaccharide hydrogels 3D printing. *International Journal of Food Science & Technology, 56*, 2264–2272. https://doi.org/10.1111/ijfs.14844

Guo, C., Zhang, M., & Devahastin, S. (2021). Improvement of 3D printability of buckwheat starch-pectin system via synergistic Ca2+−microwave pretreatment. *Food Hydrocolloids, 113*, Article 106483. https://doi.org/10.1016/j.foodhyd.2020.106483

Herranz, B., Criado, C., Angeles Pozo-Bayon, M., & Dolores Alvarez, M. (2021). Effect of addition of human saliva on steady and viscoelastic rheological properties of some commercial dysphagia-oriented products. *Food Hydrocolloids, 111*, Article 106403. https://doi.org/10.1016/j.foodhyd.2020.106403

Jeon, E., Chun, Y., & Kim, B.-K. (2023). Investigation of carrot/squid blends as edible inks for extrusion 3D printing: Effect of hydrocolloids incorporation. *Journal of Food Engineering, 364*, Article 111777. https://doi.org/10.1016/j.jfoodeng.2023.111777

Klost, M., & Drusch, S. (2019). Structure formation and rheological properties of pea protein-based gels. *Food Hydrocolloids, 94*, 622–630. https://doi.org/10.1016/j.foodhyd.2019.03.030

Nonappa, & Kolehmainen, E. (2016). Solid state NMR studies of gels derived from low molecular mass gelators. *Soft Matter, 12*, 6015–6026. https://doi.org/10.1039/C6SM00969G

Krystyjan, M., Dobosz-Kobędza, A., Sikora, M., & Baranowska, H. (2022). Influence of xanthan gum addition on the short- and long-term Retrogradation of corn starches of various amylose content. *Polymers, 14*, 452. https://doi.org/10.3390/polym14030452

Li, L., Zhang, M., & Yang, P. (2019). Suitability of LF-NMR to analysis water state and predict dielectric properties of Chinese yam during microwave vacuum drying. *LWT-*

FOOD SCIENCE AND TECHNOLOGY, 105, 257–264. https://doi.org/10.1016/j.lwt.2019.02.017

Li, P., Zhang, X. X., Li, S. K., Du, G. R., Jiang, L. W., Liu, X., & Shan, Y. (2020). A rapid and nondestructive approach for the classification of different-age Citri Reticulatae Pericarpium using portable near infrared spectroscopy. *Sensors, 20*, 16. https://doi.org/10.3390/s20061586

Liu, L., & Ciftci, O. (2020). Effects of high oil compositions and printing parameters on food paste properties and printability in a 3D printing food processing model. *Journal of Food Engineering, 288*, Article 110135. https://doi.org/10.1016/j.jfoodeng.2020.110135

Liu, Z., Bhandari, B., Guo, C., Zheng, W., Cao, S., Lu, H., & Li, H. (2021). 3D printing of shiitake mushroom incorporated with gums as dysphagia diet. *Foods, 10*, Article 2189. https://doi.org/10.3390/foods10092189

Liu, Z., Bhandari, B., Prakash, S., Mantihal, S., & Zhang, M. (2018). Linking rheology and printability of a multicomponent gel system of carrageenan-xanthan-starch in extrusion based additive manufacturing. *Food Hydrocolloids, 87*, 413–424. https://doi.org/10.1016/j.foodhyd.2018.08.026

Liu, Z., Zhang, M., & Bhandari, B. (2018). Effect of gums on the rheological, microstructural and extrusion printing characteristics of mashed potatoes. *International Journal of Biological Macromolecules, 117*, 1179–1187. https://doi.org/10.1016/j.ijbiomac.2018.06.048

Liu, Z., Zhang, M., & Ye, Y. (2020). Indirect prediction of 3D printability of mashed potatoes based on LF-NMR measurements. *Journal of Food Engineering, 287*, Article 110137. https://doi.org/10.1016/j.jfoodeng.2020.110137

Luo, H., Guo, C., Lin, L., Si, Y., Gao, X., Xu, D., & Yang, W. (2020). Combined use of rheology, LF-NMR, and MRI for characterizing the gel properties of Hairtail surimi with potato starch. *Food and Bioprocess Technology, 13*, 637–647. https://doi.org/10.1007/s11947-020-02423-y

Maniglia, B. C., Lima, D. C., da Matta Junior, M., Oge, A., Le-Bail, P., Augusto, P. E. D., & Le-Bail, A. (2020). Dry heating treatment: A potential tool to improve the wheat starch properties for 3D food printing application. *Food Research International, 137*, Article 109731. https://doi.org/10.1016/j.foodres.2020.109731

McClements, D. (2021). Food hydrocolloids: Application as functional ingredients to control lipid digestion and bioavailability. *Food Hydrocolloids, 111*, Article 106404. https://doi.org/10.1016/j.foodhyd.2020.106404

Ozel, B., Uguz, S. S., Kilercioglu, M., Grunin, L., & Oztop, M. H. (2017). Effect of different polysaccharides on swelling of composite whey protein hydrogels: A low field (LF) NMR relaxometry study. *Journal of Food Process Engineering, 40*, Article e12465. https://doi.org/10.1111/jfpe.12465

Piyush Kumar, R., & Kumar, R. (2020). 3D printing of food materials: A state of art review and future applications. Materials Today Proceedings, 33, 1463–1467. https://doi.org/https://doi.org/10.1016/j.matpr.2020.02.005.

Saha, D., & Bhattacharya, S. (2010). Hydrocolloids as thickening and gelling agents in food: A critical review. *Journal of Food Science and Technology, 47*, 587–597. https://doi.org/10.1007/s13197-010-0162-6

Sugiharto, K., Rahman, A.N.F., & Zainal (2020). The effect of solvent type and extraction duration on purple corn anthocyanin compounds (Zea Mays L). IOP Conference Series: Earth and Environmental Science, 486, 012055. doi:https://doi.org/10.1088/1755-1315/486/1/012055.

Wilson, S. A., Cross, L. M., Peak, C. W., & Gaharwar, A. K. (2017). Shear-thinning and Thermo-reversible Nanoengineered inks for 3D bioprinting. *ACS Applied Materials & Interfaces, 9*, 43449–43458. https://doi.org/10.1021/acsami.7b13602

Yang, F., Zhang, M., Bhandari, B., & Liu, Y. (2017). Investigation on lemon juice gel as food material for 3D printing and optimization of printing parameters. *LWT - Food Science and Technology, 87*, 67–76. https://doi.org/10.1016/j.lwt.2017.08.054

Yang, F., Zhang, M., & Liu, Y. (2018). Effect of post-treatment microwave vacuum drying on the quality of 3D-printed mango juice gel. *Drying Technology, 37*, 1–9. https://doi.org/10.1080/07373937.2018.1536884

Yu, H.-Z., Chi, S.-Y., Li, D., Wang, L.-J., & Wang, Y. (2022). Effect of gums on the multi-scale characteristics and 3D printing performance of potato starch gel. *Innovative Food Science & Emerging Technologies, 80*, Article 103102. https://doi.org/10.1016/j.ifset.2022.103102

Zhang, W., Cheng, S., Wang, S., Yi, K., Sun, S., Lin, J., & Li, D. (2021). Effect of pre-frying on distribution of protons and physicochemical qualities of mackerel. *Journal of the Science of Food and Agriculture, 101*, 4838–4846. https://doi.org/10.1002/jsfa.11130

Zhu, N., Wang, K., Zhang, S.-l., Zhao, B., Yang, J.-n., & Wang, S.-w. (2021). Application of artificial neural networks to predict multiple quality of dry-cured ham based on protein degradation. Food Chemistry, 344, 128586. doi:https://doi.org/10.1016/j.foodchem.2020.128586.

Zhu, S., Stieger, M. A., Van der Goot, A. J., & Schutyser, M. A. I. (2019). Extrusion-based 3D printing of food pastes: Correlating rheological properties with printing behaviour. *Innovative Food Science & Emerging Technologies, 58*, Article 102214. https://doi.org/10.1016/j.ifset.2019.102214